Macromolecules

pubs.acs.org/Macromolecules Article

Water-Stable Thin-Film Nanostructures from Amphiphilic Cationic Bottlebrush Block Copolymers by Grafting-through Ring-Opening Metathesis Polymerization

Hathaithep Senkum, Peter V. Kelly, and William M. Gramlich*

Cite This: *Macromolecules* 2021, 54, 7987−7997 Read Online

ACCESS | Metrics & More | Article Recommendations | Supporting Information

ABSTRACT: Well-defined and densely grafted amphiphilic cationic bottlebrush block copolymers (BBCPs) containing polystyrene (PS) and quaternary ammonium polymer (PDMH) side chains, PS-*b*-PDMH, were successfully generated from grafting-through ring-opening metathesis polymerization. The amphiphilic BBCP thin films, analyzed by atomic force microscopy (AFM), could self-assemble into distinct nanometer-scale domains of which the morphologies were manipulated by the volume fraction of the cationic block (f_{PDMH}), degree of polymerization, and asymmetric block side-chain lengths. The morphological stability of the BBCP thin films upon water exposure was investigated. The AFM images of casted BBCP films demonstrated surface roughening and morphology changes upon submersion as compared to precursor dry films, which was attributed to the swelling of the cationic domains and the rearrangement of the alkyl chain pendant groups under water. Thermally annealed films of PS-*b*-PDMH with an f_{PDMH} of 0.5 exhibited water-stable surfaces after water submersion, indicating that the BBCP structure can prevent some surface rearrangement. Such coatings could be used as potential antimicrobial and antifouling surfaces in future studies.

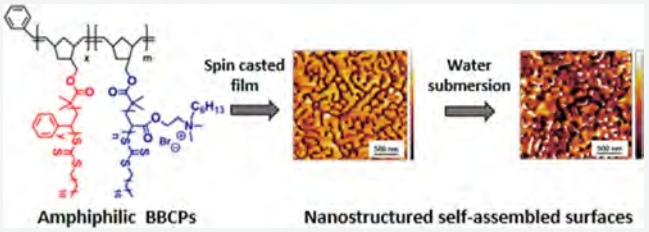

INTRODUCTION

Block copolymers (BCPs) have attracted considerable attention due to their self-assembly into nanostructures,[1,2] leading to various useful applications as drug carriers,[3] stimuli-responsive materials,[4] ion-exchange membranes,[5] and anti-biofouling coatings.[6,7] The self-assembled behaviors and sizes can be tuned by the volume fraction (f), total degree of polymerization (DP) (N), and the Flory−Huggins interaction parameter (χ).[8,9] Linear BCPs with molecular weights (MWs) of 10−100 kg/mol spontaneously phase-segregate into 10−40 nm domains.[10,11] Creating larger domains (>100 nm) from linear BCPs is challenging due to difficult polymer synthesis and high chain entanglement. Unlike linear BCPs, bottlebrush BCPs (BBCPs) with densely grafted side chains for each block can overcome these limitations to generate large nanodomains due to their extended polymer architectures.[12] The tunable phase-separated morphologies and domain sizes are dictated by side-chain lengths and symmetries of the polymer branches since they directly affect the molecular packing and interfacial curvature.[13,14] The interfacial curvature becomes small for BBCPs with symmetric side chains but becomes larger with asymmetric side-chain lengths in the blocks.[15] Thus, side-chain length asymmetry has emerged as a method to tune BBCP phase separation morphologies.

Thin nanometer-scale-structured surface coatings are one area that BBCPs have attracted interest due to their assessable domain sizes. These films include amphiphilic coatings that can be created from self-segregated surfaces of BCPs containing a hydrophilic block covalently bound to a hydrophobic block.[16] These coatings are interesting for antimicrobial[17,18] and antimarine fouling purposes[19] due to relatively low toxicity and higher antifouling efficiency compared to low-MW biocides.[18] These amphiphilic thin films and nanostructured surfaces can rearrange and change structure upon water exposure as evidenced by morphology and domain sizes changes.[16,20,21] For example, Cho et al. created triblock copolymers containing a hydrophobic aliphatic group combined with hydrophilic poly(ethylene glycol) (PEG).[21] Higher PEG content polymers had more morphological rearrangement and domain swelling after submersion in water. Additionally, Martinelli et al. reported significant transformation of well-ordered morphologies in the dry film to mixed surface structures in wet films despite forming the coating from comb-like BCPs.[20] Such an alteration of surface structures from different environments originates from the flexibility of linear BCPs or comb-like polymers. Thus, the sterically hindered conformations of BBCPs could presumably

Received: May 31, 2021
Revised: August 4, 2021
Published: August 18, 2021

https://doi.org/10.1021/acs.macromol.1c01161
Macromolecules 2021, 54, 7987−7997

Scheme 1. Amphiphilic Cationic Bottlebrush Block Copolymerization by Sequential ROMP of Polystyrene MMs (NB-PS) and Quaternary Ammonium MMs (NB-PDMH)

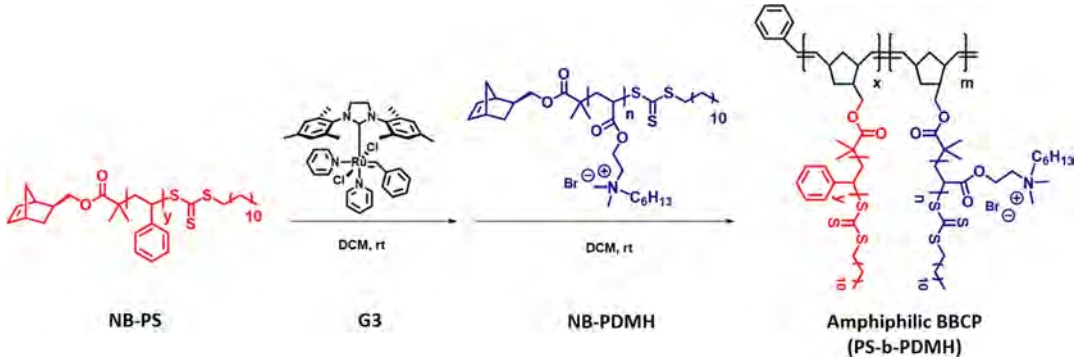

maintain surface morphologies when environmental changes occur. Preserving the original dry state morphology should improve connecting and predicting how morphological structure properties lead to macroscale behavior.

BBCP films have been employed for antimicrobial applications,[22,23] and the prevalent functional groups used in this field are quaternary ammonium groups that act as contact-killing polymers.[24,25] The electrostatic interaction between the quaternary ammonium groups and the negative charges of a bacteria's cell wall causes cell rupture and cell death. The direct synthesis of well-defined, densely grafted amphiphilic BBCPs carrying cationic functional groups is challenging due to selecting a solvent to keep both blocks soluble. An alternative method is the postpolymerization modification of precursor BCPs to yield polymers with the charged blocks; however, this process can lead to incomplete modification and lower side-chain density.[26−28] Although direct creation of BBCPs with a high density of charged constituents in the polymer chains is challenging, our recent publication reported the first successful methodology to synthesize well-defined BBCPs by a grafting-through approach, yielding a densely charged macromolecular brush.[29] These amphiphilic BBCPs were hypothesized to be able to form phase-separated morphologies in thin films and that their BBCP structure would reduce morphological changes after water submersion.

Herein, we report a technique to synthesize amphiphilic BBCPs containing dense side chains of quaternary ammonium groups by sequential grafting-through ring-opening metathesis polymerization (ROMP). As briefly demonstrated in a previous publication,[29] sequential ROMP of norbornene-capped polystyrene macromonomers (PS-MM) and norbornene-functionalized quaternary ammonium macromonomers (MMs) with six-carbon pendant groups afforded well-defined amphiphilic BBCPs with low dispersity (Scheme 1). In this work, a library of these BBCPs was synthesized to explore the thin-film phase behaviors by atomic force microscopy (AFM) in response to different block volume fractions, symmetries of side chains, and total DPs. The stability of the morphologies was examined upon water exposure, and the morphology could be stabilized by thermal annealing prior to water submersion. Understanding the nanometer-scale phase behaviors of these polymers and their stability widens opportunities for developing potential candidates for antifouling materials and other applications where cationic charges are important.

EXPERIMENTAL SECTION

Materials. All chemicals and solvents were purchased from commercial sources and used as received unless otherwise noted. Inhibitors were removed from styrene (St) and 2-(dimethylamino)-ethyl acrylate by passing through a basic alumina column and vacuum distillation prior to use, respectively. Inhibitor-free anhydrous tetrahydrofuran, ACS-grade methylene chloride (DCM), and ethyl vinyl ether (EVE) were used as received. The third-generation Grubbs catalyst, $(H_2IMes\text{-}pyr)_2(Cl)_2RuCHPh$ (G3), polystyrene (NB-PS) with DPs of 17 and 39, and norbornene-functionalized poly-(dimethylhexyl bromo)ethyl acrylate (NB-PDMH) with a DP of 14 were synthesized according to the previously reported procedures.[29]

Characterization. Number-average MW (M_n) and dispersity values ($Đ$) were obtained from size exclusion chromatography (SEC) analysis using a 1260 Agilent Chromatograph, three Phenogel (Phenomenex) columns in series with pore sizes of 50, 10^3, and 10^6 Å, and a refractive index detector with linear polystyrene (PS) standards. SEC analysis was performed using a mobile phase of dimethylformamide (DMF) containing 0.5 wt % LiBr salt, filtered through a 0.45 μm polypropylene membrane before use, with a flow rate 1.0 mL min^{-1} at 70 °C. ^1H NMR spectra were obtained using a Bruker AVANCE NEO 500 MHz spectrometer in deuterated chloroform ($CDCl_3$). DSC was performed on a TA Instruments 2500 to determine the glass transition temperature (T_g) of the bottlebrush polymers. Approximately, 2.0 mg of samples was heated under a nitrogen atmosphere over a temperature range of 0−160 °C at a ramp rate of 10 °C/min using a heat/cool/heat cycle. The T_g was reported from the second heating data. Water contact angles were measured with a mobile surface analyzer (Krüss) using 1 μL droplet of water at 20 °C. Prior to measurement, the water droplet was equilibrated on the polymer thin films for 60 s. The reported data were derived from six analyzed spots of two replicate samples and then averaged using the measured angles from the left and the right side of the droplet. AFM was performed on an Asylum Research MFP-3D microscope to analyze the surface topographies (height images) and morphologies (phase images) of the polymer films through the tapping mode, using silicon cantilevers (model of AC160TS-R3 received from OXFORD instruments) with a resonant frequency of 300 kHz, a spring constant of 26 N/m, and a silicon tip radius of 7 nm. Images of 2 × 2 μm^2 were captured in the tapping mode at the set amplitude equal to 25% of the drive amplitude, at a 0.5 Hz scan rate, with 192 scan points and lines per image. The polymer films were kept under vacuum prior to AFM characterization. Domain spacings (d-spacing) were determined by computing the phase images in Gwyddion software (version 2.54) through a radial power spectral density function (radial PSDF) to provide a plot of the radial average in terms of intensity (y-axis) versus distance (nm^{-1}). Then, the plot was fit by a Lorentzian function to provide a q-value as the maximum intensity of the fit curve. The q-values were used in the equation $L_0 = \frac{2\pi}{q}$ to evaluate the domain spacing (L_0, nm scale) of the phase-separated BBCPs.[26,30] The domain spacing was measured

https://doi.org/10.1021/acs.macromol.1c01161
Macromolecules 2021, 54, 7987−7997

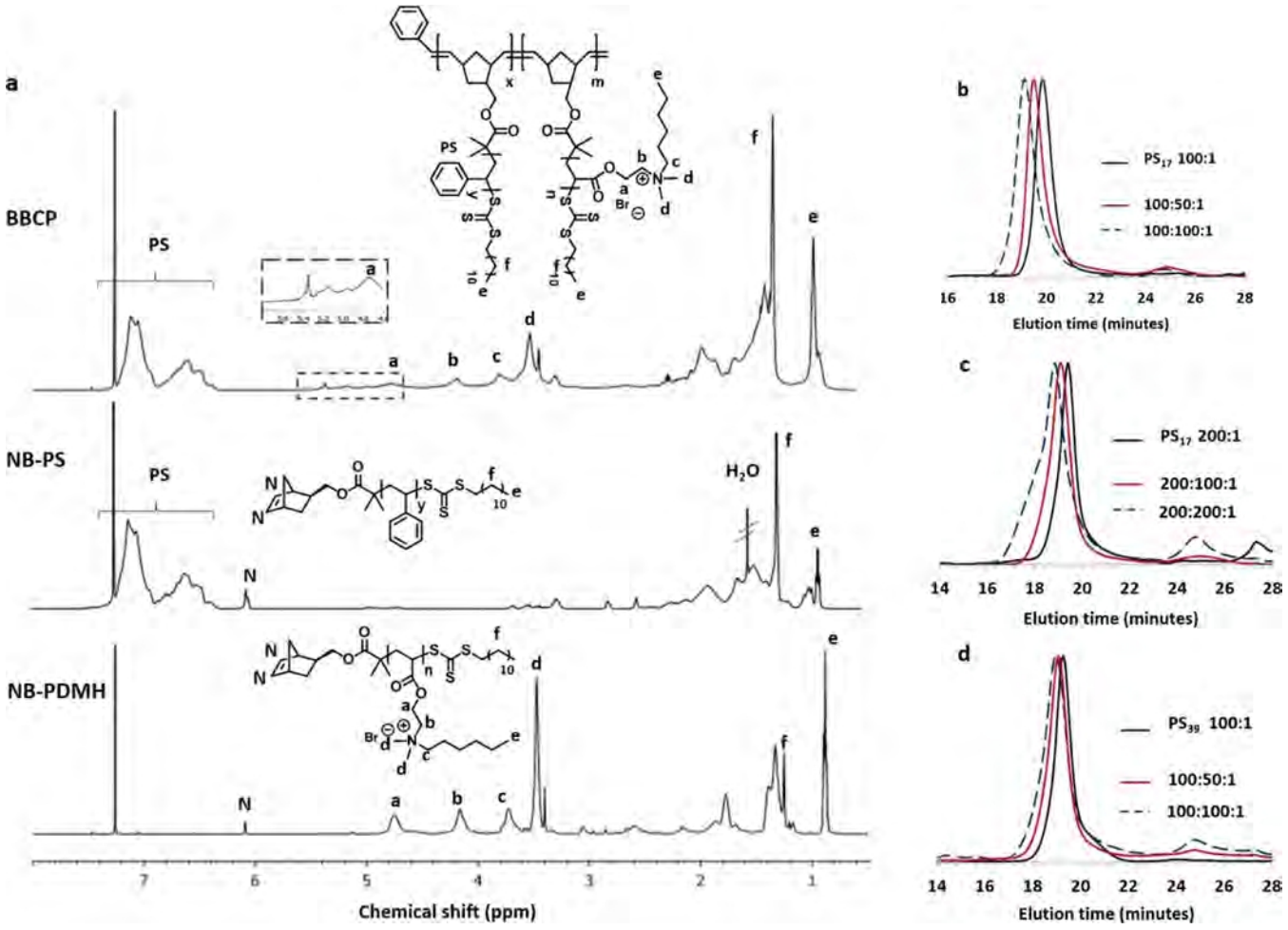

Figure 1. (A) ^{1}H NMR spectra of norbornene-functionalized quaternary ammonium MM of NB-PDMH (14 DP), norbornene-functionalized PS of NB-PS$_{17}$ (17 DP), and precipitated BBCP of PS$_{17}$-*b*-PDMH with a DP molar ratio for PS/NB-PDMH/G3 of 200:100:1. (B) SEC curves of BBCPs of PS$_{17}$-*b*-PDMH using NB-PS$_{17}$ macroinitiators with ratios of NB-PS$_{17}$/G3 of 100:1 which is referred to as PS$_{17}$ 100:1. Molar ratios of PS to PDMH to G3 are given as ###:###:1. (C) SEC curves of BBCPs of PS$_{17}$-*b*-PDMH using NB-PS$_{17}$ macroinitiators with ratios of NB-PS$_{17}$/G3 of 200:1 which is referred to as PS$_{17}$ 200:1. (D) SEC curves of BBCPs of PS$_{39}$-*b*-PDMH from NB-PS$_{39}$ macroinitiators with ratios of NB-PS$_{39}$/G3 of 100:1 which is referred to as PS$_{39}$ 100:1.

for four different AFM phase images over regions over 2 × 2 μm^2 and averaged to provide average domain spacing values and standard deviation. The root-mean square of the surface roughness (R_{rms}) was determined from AFM height images.

Synthesis of Amphiphilic BBCPs of PS-*b*-PDMH by ROMP. In a general procedure for amphiphilic bottlebrush block polymerization via ROMP, all vials, stir bars, and syringes were dried before use and ROMP was undertaken in a glove bag under a N_2 atmosphere. The desired amounts of NB-PS and NB-PDMH MMs were prepared in separate 4 mL vials equipped with a stir bar and rubber septa cap and then purged with nitrogen gas for 30 min. A 20 mL ampule with 10 mL of DCM was degassed by three freeze−pump−thaw cycles prior use. In an experimental example for ROMP of PS$_{17}$-*b*-PDMH with a NB-PS$_{17}$/NB-PDMH/G3 of 50:50:1 in a glove bag, 0.28 mL of DCM was added to the individual vials to prepare the 0.05 M MM solution using an airtight glass syringe. Then, 0.2 mL of freshly prepared G3 solution (1 mg/mL in DCM, 0.0002 g, 2.75 × 10^{-4} mmol) was added to the vial containing NB-PS solution to start homopolymerization, which ran for 6 min. After this time, an aliquot of the crude of bottlebrush PS was extracted and then quenched with 0.3 mL of EVE in 0.6 mL of DCM (33% v/v). The NB-PDMH MM solution was sequentially added into the remaining bottlebrush PS solution by a N_2-purged syringe to continue block copolymerization, which was run for 2 h. ROMP reactions were quenched by adding EVE solution in DCM (33% v/v) to the reaction vial. All crude samples were purged with N_2 gas to eliminate excess EVE and then dried in a vacuum oven at 45 °C for 2 days to remove the remaining EVE before being analyzed by ^{1}H NMR spectroscopy in $CDCl_3$ and SEC to find % MM conversion, M_n, and dispersity. For other polymerizations, the same procedures were performed at the same concentrations of MM and G3 solutions using the calculated amount of starting materials corresponding to the desired mole ratios of NB-PS to NB-PDMH to G3. Polymerizations were run to achieve at least 95% conversion of NB-PDMH. The BCPs were purified by precipitation into dry-ice-chilled diethyl ether from DCM twice and then precipitated into dry-ice-chilled diethyl ether from chloroform twice. The precipitate in diethyl ether was collected by centrifugation and then dried in a vacuum oven. The DP of each block in a copolymer was determined from monomer conversions because peak overlap in the ^{1}H NMR spectra prevented selection of an end group internal reference. These DP values for each block were then used to calculate the volume fraction of PDMH (f_{PDMH}).

Polymer Film Preparation. Glass slides were cleaned by immersion and sonication in a sequence of solvents, reverse osmosis (RO) water, acetone, and isopropanol, for 1 h and then dried in a vacuum oven overnight. BBCP solutions were prepared in chloroform ($CHCl_3$) at a 20 mg/mL concentration by stirring for 30 min before being filtered through a 0.20 μm syringe filter. The filtered polymer solutions (100 μL solution) were spin-coated onto the cleaned glass slides with a spin rate of 1500 rpm for 30 s and then 500 rpm for

https://doi.org/10.1021/acs.macromol.1c01161
Macromolecules 2021, 54, 7987−7997

Table 1. PS-*b*-PDMH BBCPs Synthesized by Sequential ROMP

entry	polymer	$[NB\text{-}PS]_0/[NB\text{-}PDMH]_0/[G3]_0$	% conversion[a]	M_n(SEC), (kg/mol)[b]	M_n(NMR), (kg/mol)[c]	$Đ$[b]	DP of PS/PDMH[c]	f_{PDMH}[d]
1	PS_{17}-*b*-PDMH	25:25:1	96	78	163	1.25	25:24	0.73
2	PS_{17}-*b*-PDMH	50:25:1	>99	120	222	1.16	50:25	0.58
3	PS_{17}-*b*-PDMH	50:50:1	97	145	329	1.24	50:48	0.73
4	PS_{17}-*b*-PDMH	100:50:1	97	160	439	1.20	100:49	0.58
5	PS_{17}-*b*-PDMH	100:100:1	98	210	661	1.23	100:98	0.73
6	PS_{17}-*b*-PDMH	200:100:1	>99	230	886	1.33	200:100	0.58
7	PS_{17}-*b*-PDMH	200:200:1	90	270	1250	1.63	200:180	0.73
8	PS_{39}-*b*-PDMH	50:100:1	>99	190	556	1.29	50:100	0.71
9	PS_{39}-*b*-PDMH	100:50:1	>99	250	443	1.25	100:50	0.40
10	PS_{39}-*b*-PDMH	100:100:1	>99	230	666	1.48	100:100	0.55

[a]% NB-PDMH conversion calculated from ^{1}H NMR spectroscopy in $CDCl_3$ from the relative integration of methylene protons at 4.76 ppm in the repeat units to norbornene protons at 6.09 ppm. [b]Obtained from SEC analysis in DMF with 0.5 wt % LiBr, RI detector, and linear PS standards. Note: since $M_{n(SEC)}$ values are relative to PS standards and the hydrodynamic behaviors of BBCPs are expected to be different than the PS standards, the reported M_n values are not the absolute MWs. [c]Determined from % NB-PDMH conversion × feed ratios of $[NB\text{-}PS]_0/[NB\text{-}PDMH]_0/[G3]_0$, with 100% conversion of NB-PS_{17} or NB-PS_{39}. [d]Volume fraction of PDMH calculated using the equation $f_{PDMH} = V_{PDMH}/(V_{PDMH} + V_{PS})$ and using the density of PDMH as 0.915 g/mL and density of PS as 1.04 g/mL, where V_{PDMH} and V_{PS} are defined as volume per mole of a polymer chain of PDMH and PS, respectively.

additional 30 s. For the thermal treatment of the spin-coated films, the freshly made films were thermally annealed in a vacuum oven at 110 °C for 17 h. Then, the films were kept under vacuum prior to AFM characterization. The polymer thickness of the unannealed film of PS_{39}-*b*-PDMH with a DP of 50:100 was measured by a cross-sectional method, as described in Supporting Information (Figures S1 and S2).

Water Submersion of BBCP Thin Films. BBCP thin films were submerged in RO water for three immersion cycles. For the first cycle of film submersion, the films were immersed under water for 3 h and transferred to dry in a vacuum oven at room temperature for 18 h. Then, films were analyzed by AFM. The second cycle was performed for 6 h with the repeated drying. Finally, the films were submerged for 3 days and dried in the vacuum oven for 10 days before being analyzed by AFM.

RESULTS AND DISCUSSION

Synthesis of PS-*b*-PDMH BBCPs. Amphiphilic bottlebrush block copolymerization was carried out by sequential grafting-through ROMP of norbornene-functionalized MMs with a highly active third-generation Grubbs catalyst (G3) in deoxygenated DCM. This technique ensured dense side chains on every repeat unit and generated architectures with controlled DPs. Prior to ROMP, MMs of NB-PS and NB-PDMH were prepared through reversible addition−fragmentation chain transfer (RAFT) polymerization using a chain transfer agent with a norbornene terminus (NB-RAFT CTA) and subsequent quaternization with 1-bromohexane to create NB-PDMH. ^{1}H NMR spectra showed that the resulting NB-PS_{17} (17 DP), NB-PS_{39} (39 DP), and NB-PDMH (14 DP) MMs could be synthesized with norbornene end groups (Figures 1A and S3). Two NB-PS were synthesized to probe how symmetry of the side-chain lengths affected the self-assembled morphology. SEC analysis demonstrated unimodal curves for all the resulting MMs with dispersity ($Đ$) below 1.3, suggesting that controlled MM structures were produced (Figure S4 and Table S1).

As previously reported, sequential polymerization of NB-PS and then NB-PDMH MMs afforded well-defined architectures of BBCPs with low $Đ$.[29] A library of BBCPs was generated by tuning the feed ratios of NB-PS to NB-PDMH to G3 (NB-PS/NB-PDMH/G3), as summarized in Table 1. ^{1}H NMR spectra showed successful ROMP of PS_{17}-*b*-PDMH as evidenced by the disappearance of the norbornenyl olefin peak (NB) at 6.07 ppm and the generation of vinyl peaks at 4.9−5.5 ppm, corresponding to the formed polynorbornene backbone (Figure 1A). This indicates an efficient initiation of PS macroinitiators with the ruthenium reactive site to further polymerize NB-PDMH by quantitative MM consumption. The ^{1}H NMR spectrum of the precipitated BBCPs proved successful sequential ROMP by incorporation of PS and cationic side chains into the macromolecular chain (Figure 1A). In this study, all BBCPs were polymerized to higher than 95% MM conversion and were then precipitated to eliminate unreacted MMs, yielding BBCPs with less than 3% impurities, which should likely not significantly impact surface morphologies.

SEC chromatograms exhibited unimodal curves ($Đ$ below 1.3) of the BBCPs clearly shifting to a shorter elution time, higher MW regions, as compared to the NB-PS macroinitiator, suggesting efficient PS-based initiation to yield well-structured BBCPs (Figure 1B,C). Larger BBCPs with higher M_n were prepared by varying the feed ratios of NB-PS/NB-PDMH/G3 and generally produced low-dispersity BBCPs. However, the BBCP with the highest feed ratio of NB-PS_{17} to NB-PDMH to G3 (200:200:1) showed a broader molecular distribution with a shoulder at higher MW and a $Đ$ of 1.63 (Figure 1C, blue dash line). This shoulder was likely due to undesirable intermolecular chain transfer occurring in the highly viscous reaction solution. The reduced diffusion rate of the reactive BBCP chains likely led to the reaction with the polynorbornene backbone of other chains rather than NB-PDMH MMs to create the shoulder.[31,32] Larger arm PS brushes (PS_{39}) also efficiently acted as macroinitiators, as demonstrated by unimodal peaks of the resulting BBCPs and low $Đ$ (Figure 1D). A library of well-defined amphiphilic BBCPs were synthesized using this method to investigate two-dimensional phase segregation, as summarized in Table 1.

Glass Transition of BBCPs. Since PS-*b*-PDMHs have not been synthesized as BBCPs previously, their glass transitions were measured to confirm the immiscible nature of the blocks and determine the temperature above which they would need to be annealed. The glass transition temperatures (T_g) of bottlebrush homopolymers of NB-PS_{17} and NB-PDMH with a DP of 100 were determined by DSC to be 69 and 34 °C, respectively (Figure S5), which are lower than reported T_g

https://doi.org/10.1021/acs.macromol.1c01161
Macromolecules 2021, 54, 7987−7997

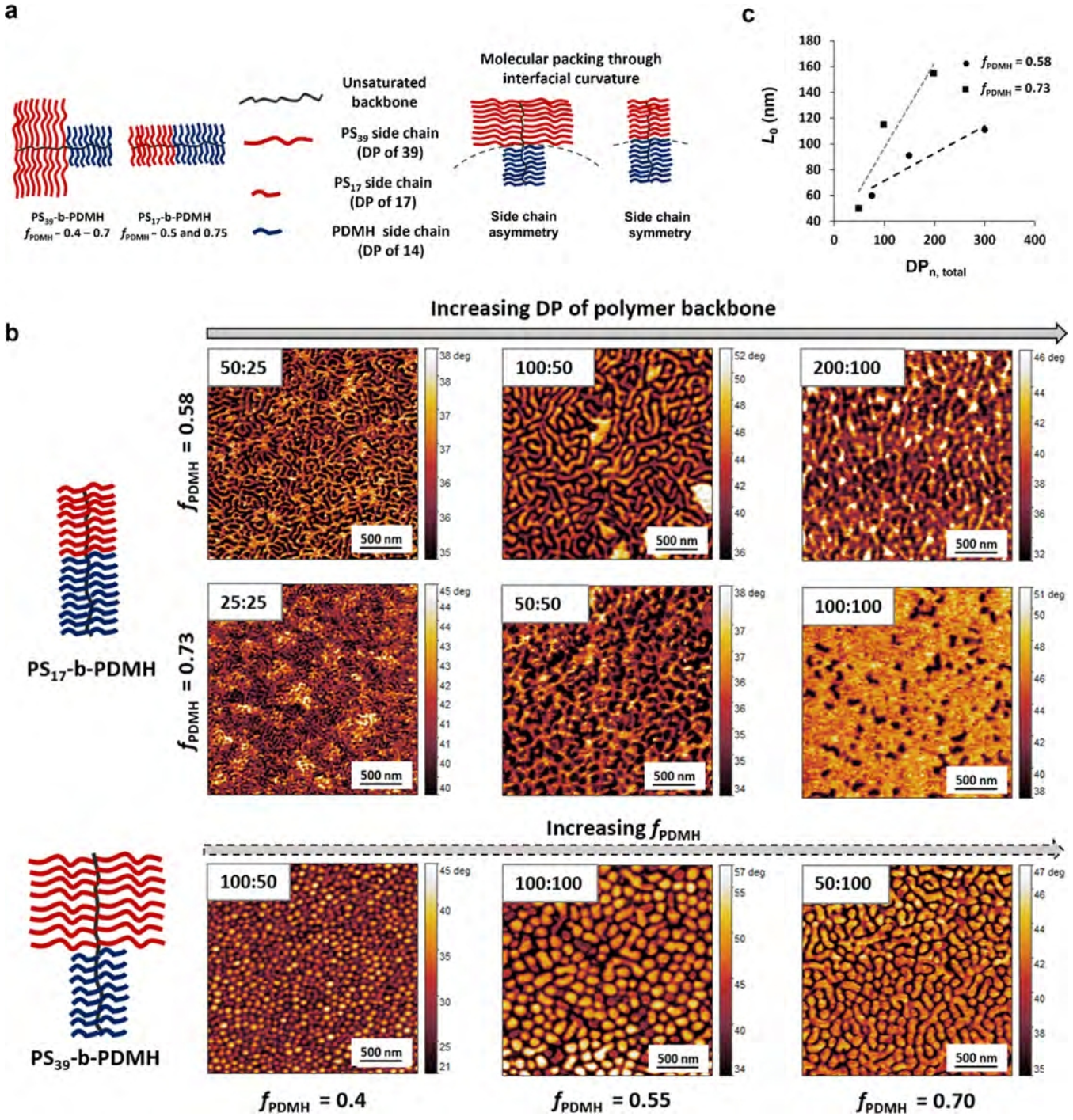

Figure 2. (A) Schematic architectures of BBCPs with varied volume fraction of PDMH (f_{PDMH}) and different side-chain lengths, yielding bottlebrushes with the side-chain asymmetry and symmetry for PS_{39}-*b*-PDMH and PS_{17}-*b*-PDMH, respectively, and a representative schematic of molecular packing through the interfacial curvature manipulated by the asymmetry of side-chain lengths and f_{PDMH}. (B) AFM phase images of PS_{17}-*b*-PDMH films (top and middle row) and PS_{39}-*b*-PDMH films (bottom row) with varied f_{PDMH} and DP of PS/PDMH. (C) Plot of domain spacing (L_0) as a function of total bottlebrush backbone length ($DP_{n\ total}$) of PS and PDMH (DP_{PS} + DP_{PDMH}) of casted films of PS_{17}-*b*-PDMH.

values for these polymers due to the low MW of the side chains.[33−35] The DSC data for BBCPs of PS_{39}-*b*-PDMH with DPs of 100 and 100 for each block demonstrated a qualitative indication that the immiscible polymers phase-separated, as evidenced by two separate T_g values corresponding to PS and PDMH (Figure S5). However, the DSC results of PS_{17}-*b*-PDMH with the same backbone DPs as PS_{39}-*b*-PDMH (100 and 100) revealed one broad T_g value at 47 °C, suggesting less well-defined regions of the two blocks (Figure S5). This result suggests that the shorter PS side chains tend to interact more with the hydrophobic six-carbon alkyl chains of the quaternary ammonium functional groups in the branches as compared to the longer side-chain PS_{39}, leading to weak segregation.[36] Nanometer-scale phase separation was still expected for the PS_{17}-*b*-PDMH polymers, but we hypothesized that the domain boundaries may be less defined and easier to rearrange when submerged in water as compared to the PS_{39}-*b*-PDMH polymers with two clear T_g values.

https://doi.org/10.1021/acs.macromol.1c01161
Macromolecules 2021, 54, 7987−7997

Table 2. Domain Spacing (L_0) of BBCP Thin Films Determined from AFM Phase Images

			L_0 of films before water submersion[a] (nm)		L_0 of films after water submersion[a] (nm)	
polymer	$[NB\text{-}PS]_0/[NB\text{-}PDMH]_0$	apparent morphology[b]	unannealed film	thermally annealed film	unannealed film	thermally annealed film
PS_{17}-*b*-PDMH	50:25	L	60 ± 2	118 ± 3	62 ± 2	128 ± 7
PS_{17}-*b*-PDMH	100:50	L	91 ± 1	184 ± 11	91 ± 1	134 ± 5
PS_{17}-*b*-PDMH	200:100	L	111 ± 3	151 ± 9	93 ± 3	137 ± 12
PS_{17}-*b*-PDMH	25:25	C	50 ± 5	64 ± 3	64 ± 4	61 ± 1
PS_{17}-*b*-PDMH	50:50	C	115 ± 9	101 ± 4	117 ± 8	86 ± 2
PS_{17}-*b*-PDMH	100:100	C	155 ± 2	146 ± 6	114 ± 10	130 ± 6
PS_{39}-*b*-PDMH	50:100	L	94 ± 1	141 ± 2	105 ± 1	128 ± 2
PS_{39}-*b*-PDMH	100:50	C	73 ± 2	183 ± 8	82 ± 3	194 ± 10
PS_{39}-*b*-PDMH	100:100	C	117 ± 3	154 ± 12	101 ± 1	114 ± 8

[a]Obtained from radial power spectral density function analysis of four different AFM phase images over two different analyzed regions on the thin films and then reported as an average ± standard deviation of the four AFM phase images. [b]Estimated by AFM phase images of casted BBCP films as determined by comparison to the similar phase-separated shapes and patterns for the BBCP in ref 38. L = perpendicular lamellae and C = perpendicular cylinder.

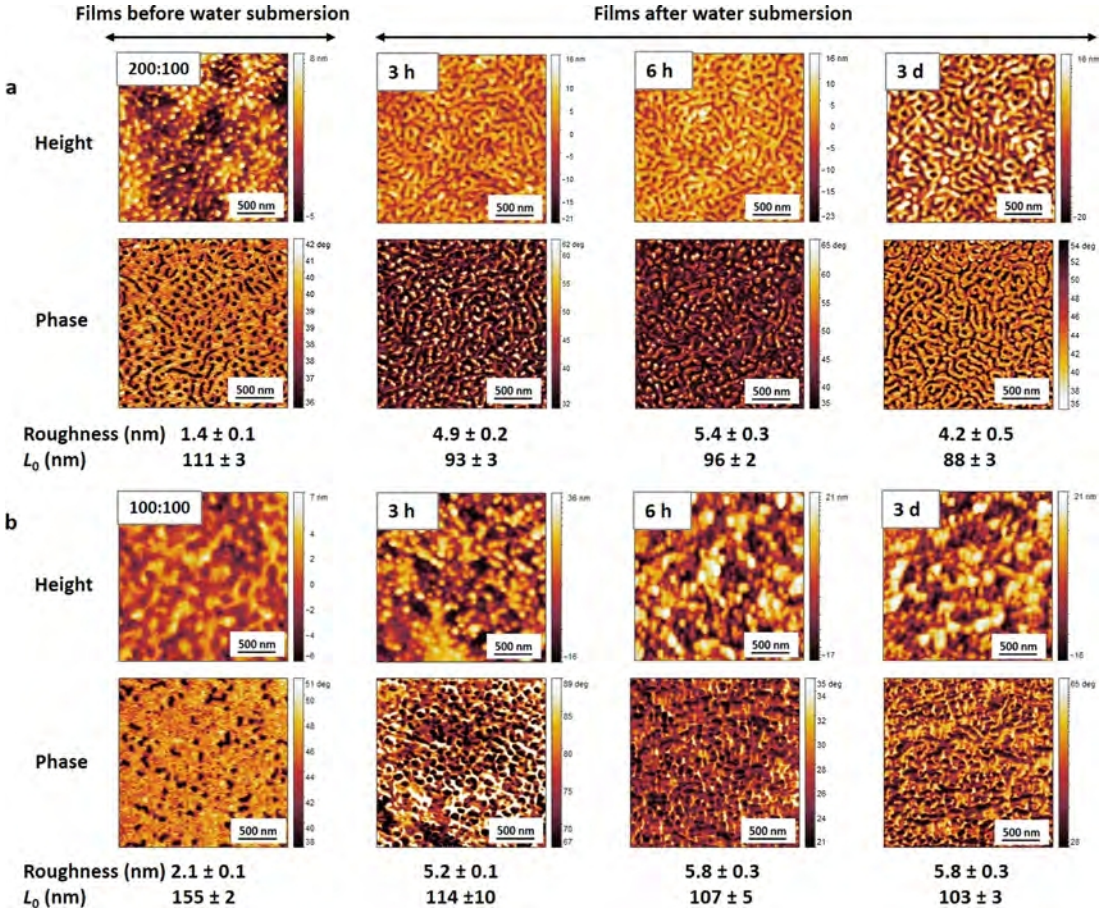

Figure 3. AFM images of films of PS_{17}-*b*-PDMH before and after three immersion cycles under water, cycle-1 for 3 h, cycle-2 for 6 h, and cycle-3 for 3 days. (A) PS_{17}-*b*-PDMH film with f_{PDMH} = 0.58 (note: phase contrast for the 3 h and 6 h sample was reduced.) and (B) PS_{17}-*b*-PDMH film with f_{PDMH} = 0.73.

BBCP Thin-Film Self-Assembly Behavior from Spin Casting. All BBCP thin films were prepared by spin casting from chloroform ($CHCl_3$) onto glass and then drying under vacuum to remove residual $CHCl_3$. Since the method of film preparation can impact phase separation of the BBCPs due to polymer−substrate interactions, polymer−atmosphere interactions, and drying rates, drying under vacuum was used to provide consistency. The coatings prepared from BBCPs with various f_{PDMH} values, overall DPs, and symmetries of the block side-chain length were characterized by AFM to explore phase separation and resultant morphology (Figure 2A). AFM phase images confirmed phase-separated self-assembly of PS and PDMH domains as evidenced by the distinct phase contrast on the surfaces (Figure 2B). Morphological changes for PS_{17}-*b*-PDMH films were observed as f_{PDMH} increased from about 0.58 to about 0.73, influencing the molecular packing shapes and interfacial curvatures (Figure 2B top and middle rows and Figures S6A and S7A). Other researchers have demonstrated that BBCPs can phase-separate into lamellar, cylindrical, or spherical morphologies, which are dependent upon the block

https://doi.org/10.1021/acs.macromol.1c01161
Macromolecules 2021, 54, 7987−7997

compositions and polymer side-chain lengths.[13,37] Our BBCP films appeared to show lamellar and cylindrical morphologies for the films with f_{PDMH} values of 0.58 and 0.73, respectively; however, definitive assignments require future scattering experiments.[38] Due to nonselective $CHCl_3$ used to cast the films and no preferential interfacial interaction between the individual block and glass surface, the self-assembled orientation exhibited perpendicular features to the surfaces.[26,39] This indicates that a balance exists between the interaction of the sterically hindered polymer brushes and the surface or the air interfaces.[39] Additionally, the high-vapor-pressure $CHCl_3$ (196.7 mm Hg) likely led to the kinetic trapping of the self-assembly due to the fast evaporation rate, favoring perpendicular orientation on the surfaces.[40] Despite the DSC data suggesting potential miscibility of the PS_{17} and PDMH, in general, domains with sharp boundaries were observed, with the 200:100 sample as the potential exception.

AFM phase images of the films with an f_{PDMH} of 0.73 and higher DP showed enrichment of the bright domain on the surface, suggesting that bright areas were the PDMH regions and dark areas were the PS segments (Figure 2B middle row).[26] Further confirmation of this assignment comes from the AFM height images where the inverse coloration is present for the morphology, giving dark PDMH and bright PS domains as the soft block and hard block, respectively (Figure S6-S8). The surface energy of a quaternary ammonium brush with a six-carbon alkyl pendant group (33 mJ m^{-2})[25] is lower than that of PS (46.8 mJ m^{-2}),[41] which explains why PDMH concentrates on the surface for an f_{PDMH} of 0.73. Furthermore, this enrichment of PDMH on the surface is consistent with its higher mobility, enabling it to migrate to the surface while drying.[25] With the asymmetric side-chain lengths of PS_{39} (DP of 39) and PDMH (DP of 14), phase behaviors revealed more circular morphology on the surface, demonstrating more curved interfaces between the domains of each block[15] (Figure 2A,B, bottom row, and Figure S8A). Morphological transitions for PS_{39}-based BBCPs were clearly noticeable as f_{PDMH} increased from 0.4 to 0.7 as bright domains began to elongate, suggesting a transition from cylinder to lamellar morphology (Figure 2B bottom row). Domain spacing (L_0) determination carried out on the AFM phase images of all coatings demonstrated larger L_0 values with increasing DP of the brush backbone as expected (Figure 2C and Table 2). As the total DP increases, the L_0 values increase linearly with the predominantly cationic BBCPs (f_{PDMH} = 0.73) increasing more significantly than those with an f_{PDMH} of 0.58, as demonstrated from the steeper slope (Figure 2C). This behavior suggests that the quaternary ammonium cations intrinsically repulse other chains and arms, thereby stretching the ionic domains.[26] These results demonstrate that the surface morphology of this new BBCP could be altered and controlled using both the side-chain asymmetry and overall polymer size.

BBCP Thin-Film Behavior after Water Submersion. Since amphiphilic surfaces often target applications in aqueous environments and surface structures can change due to structural reorganization of the polymer segments under water, the stability of the morphology after water submersion was studied.[42] Although some regions of the self-assembled films detached during water exposure, most of the film remained attached and the phase separation of the thin films was still evidently visible and analyzable by AFM. PS_{17}-*b*-PDMH films with DPs of 200:100 (f_{PDMH} = 0.58) and 100:100 (f_{PDMH} = 0.73) were submerged under water for three cycles. After the initial water submersion, AFM height images of the films demonstrated a significant roughness increase as compared to the dry state and did not change for subsequent cycles (Figure 3A,B, top images). This trend was attributed to swelling of the charged polymer segments (PDMH) when under water.[43] AFM phase images of the films after water submersion also exhibited features of swelling and morphological changes after the initial submersion but did not change after subsequent submersions (Figure 3A,B, bottom images). This stability over subsequent submersions suggested that the surface reached an equilibrium under water after the initial submersion cycle. The PS regions appeared below the PDMH domains, which is consistent with these hydrophobic domains minimizing interfacial contact with water. Additionally, the domain spacing (L_0) values of the BBCP films decreased after initial water submersion and then tended to be constant for subsequent submersions (Figure 3 and Table 2). These results are consistent with He et al., which demonstrated that the long alkyl chain groups of quaternary ammonium polymers that were grafted from silica oxide surfaces rearranged to inside the brush block polymer chains to avoid unfavorable interfacial energy from contacting water.[43] The significant reduction in L_0 values for a BBCP with an f_{PDMH} of 0.73 may result from migration of the more hydrophobic six-carbon alkyl groups of the PDMH segment into the PS domains underneath the PDMH regions, causing only the methyl groups of the ammonium to stay exposed to the surface and, thus, reducing the macromolecular extension of the BBCP backbone off the surface. The aggregation could promote the exposure of the positively charged moieties to the water surface, supporting the rough surfaces.[43] Since the morphology of BBCP films seemed to not change after the initial submersion cycle, other BBCP films of PS_{17}-*b*-PDMH (f_{PDMH} of 0.58) with DPs of 100:50 and 50:25 and BBCP films of PS_{39}-*b*-PDMH (f_{PDMH} of 0.40) with a DP of 100:50 were imaged only after the initial submersion cycle. The similar trends of the swelling PDMH features and morphology change were observed in the AFM phase images (Figures S9 and S10A), which indicates that water contact can change the nanometer scale to some extent, which was expected. Interestingly, the domain spacing typically only changed 10−20 nm, indicating that the overall morphology of these samples was somewhat stable. As a comparison to another representative water-soluble polymer, Cho et al. reported that the domain sizes of self-assembled thin films of a triBCP grafted with amphiphilic side chains containing hydrophilic polyethylene glycol (PEG) and PS significantly changed by 40−150 nm after water submersion due to the swelling of hydrophilic PEG in water.[21,48] This suggests that the sterically hindered bottlebrush structures could help mitigate domain size changes under water.

BBCP Thin-Film Behavior after Thermal Annealing. One of the factors governing the self-organization of BBCPs was likely the solvent evaporation rate from each domain, which consequently kinetically influences the phase segregation. This approach led the BBCPs to likely not obtain equilibrium phase structures. Thermal annealing above the T_g of both polymers (110 °C for 17 h) prior to AFM analysis attempted to equilibrate the films after spin coating. After annealing, AFM images revealed somewhat different morphological features as demonstrated by larger phase separated domains on the surfaces as compared to the BBCP films as casted (Figures S6B− S8B). The L_0 values of thermally annealed films were also significantly larger than that of casted

https://doi.org/10.1021/acs.macromol.1c01161
Macromolecules 2021, 54, 7987−7997

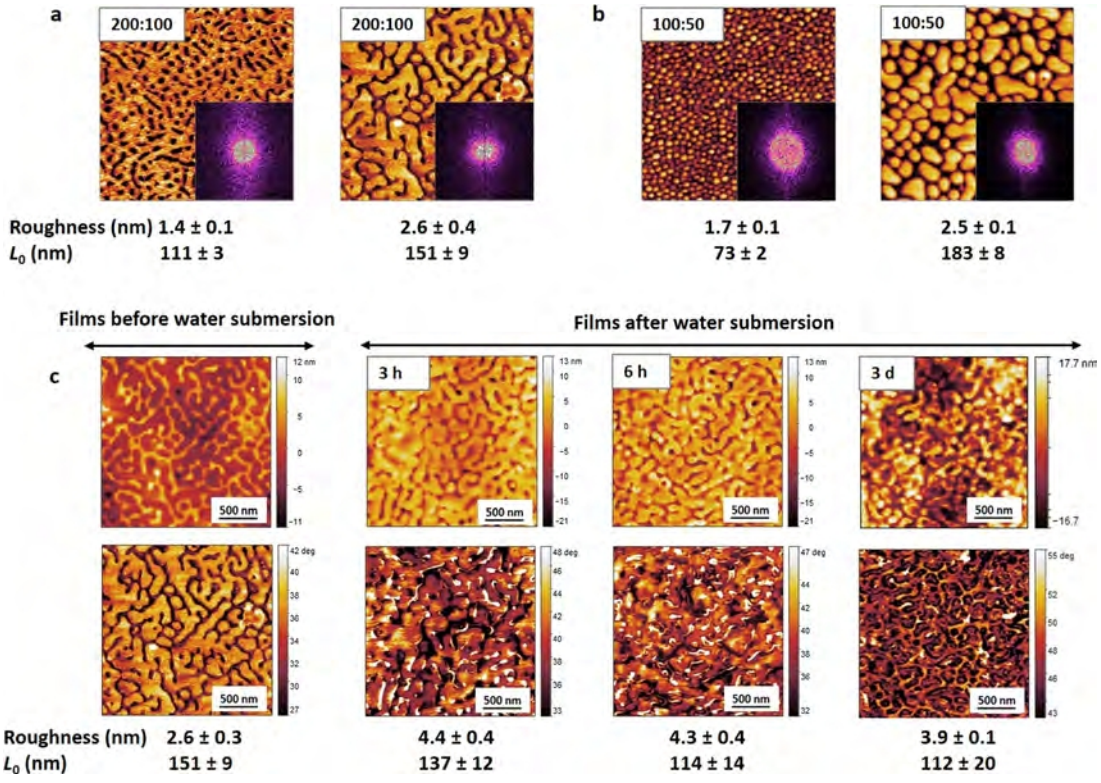

Figure 4. (A) AFM images and inset FFT images of BBCP films of PS_{17}-*b*-PDMH with 200:100 prepared by the nonannealing method (the left image) and thermal annealing method (the right image). (B) AFM images and its FFT images of BBCP films of PS_{39}-*b*-PDMH with 100:50 prepared by the nonannealing method (the left image) and thermal annealing method (the right image). (C) AFM height images (top) and phase images (bottom) of thermally annealed films of PS_{17}-*b*-PDMH with f_{PDMH} = 0.58 and DP of PS/PDMH of 200:100 before and after water submersion over three submersion cycles.

films. The L_0 values of the thermally annealed films for f_{PDMH} = 0.73 remained linear as a function of the polymer backbone DP. However, for an f_{PDMH} of 0.58 (Figure S11b), the L_0 changed less as a function of total DP. This suggests that the thermal annealing tended to induce thermodynamic phase separation of the blocks on the macromolecular brushes (Table 2).[44] The morphology of the thermally annealed film did not change despite a longer annealing time (21 h), suggesting that 17 h thermal annealing was long enough to equilibrate the BBCP films (Figure S12). Fast Fourier transform (FFT) of AFM phase images was utilized to evaluate the extent that the morphology was ordered, since higher ordered nanostructures are expected to yield sharper contrast of the FFT circles.[45] FFT images of annealed films showed a more discrete center than that of unannealed films, suggesting that the heating allowed the BBCPs to phase separate into more stable and ordered features (Figure 4A,B). The increased order and domain spacing indicated that thermal annealing can be used to a closer approach an equilibrium structure that was not kinetically trapped by the solvent evaporation process.

Since thermal annealing appeared to enable the morphology to more closely approach equilibrium, we hypothesized that these morphologies would be more stable through water submersion. After three cycles of water submersion, the thermally annealed PS_{17}-*b*-PDMH films with a DP of 200:100 (f_{PDMH} = 0.58) exhibited a stable morphology despite the increasing surface roughness from swelling of the PDMH domains (Figure 4C, top images and Table S2). Additionally, the surface roughness of annealed films increased less after submersion than the roughness of unannealed films upon submersion. These results supported that thermal annealing created more stable morphological patterns driven by thermodynamic phase separation. The L_0 values for BBCP films did decrease after initial submersion, which was likely due to the swelling of PDMH segments (Figure 4C, bottom images and Table 2). Additionally, the correlation between the L_0 values and total DP of the brush backbone of the thermally annealed films after water submersion still had a linear trend without a significant difference as compared to the annealed films (Figure S11). Similarly, the thermally annealed films of PS_{39}-*b*-PDMH (f_{PDMH} of 0.40) with a DP of 100:50 exhibited a consistent phase-separated morphology and slight increase in the surface roughness after initial water submersion for 3 h (Figure S10B). The thermally annealed films of PS_{17}-*b*-PDMH with a DP of 100:100 and higher f_{PDMH} (f_{PDMH} of 0.73) had swollen features accompanied with gradually roughening surfaces and changing morphology after three submersion cycles (Figure S13 top). After initial submersion, AFM images showed the slightly swollen pattern of the PDMH domains on the surface and the spherical domains of PS showed aggregation underneath the swelling PDMH domains. After three submersion cycles, the spherical regions became larger and more noticeable on the surfaces, whereas the L_0 values decreased (Figure S13, bottom). This occurrence was likely due to more aggregation of alkyl pendant groups of PDMH polymer segments and the long alkyl chain of RAFT CTA after being submerged longer. Likewise, such morphology changes and significant reduction of the L_0 values were clearly observed on the BBCP films of P_{S39}-*b*-PDMH with a DP of 50:100 (f_{PDMH} = 0.70) after the initial submersion process for 3 h

https://doi.org/10.1021/acs.macromol.1c01161
Macromolecules 2021, 54, 7987−7997

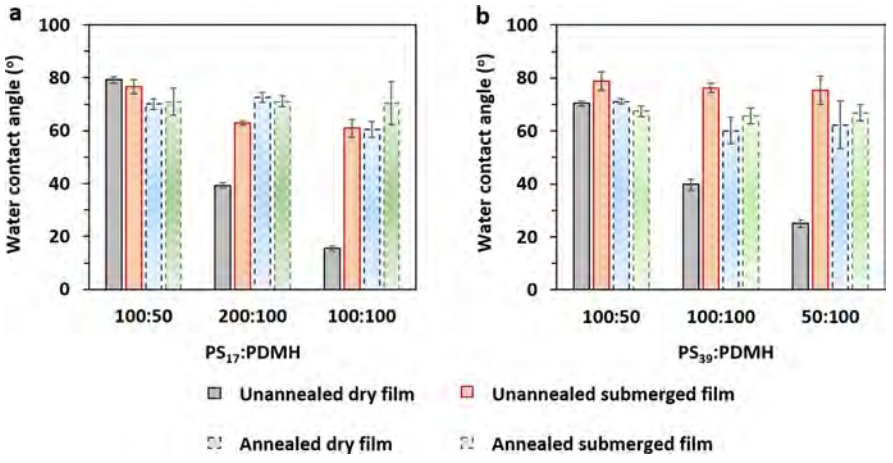

Figure 5. Water contact angle (deg) for different DPs of PS/PDMH unannealed and thermally annealed films before and after water submersion for 3 h. (A) BBCP films of PS_{17}-*b*-PDMH and (B) BBCP films of PS_{39}-*b*-PDMH.

(Figures S14 and S15). This suggests that the BBCP films containing predominantly cationic domains are more likely to undergo structural reorganization of the polymers under water despite the obtained equilibrium morphology in the dry state.

In addition to AFM analysis, static water contact angles were measured to evaluate the wettability of some BBCP films before and after water submersion (Figure S16), which can serve as an indicator whether significant changes were occurring to the film surface. Before water submersion, most of the unannealed BBCP films exhibited hydrophilic surfaces as demonstrated by a low water contact angle (25−40°), while the thermally annealed films had higher water contact angles (60−70°) (Figure 5 and Table S2).[44] After water submersion, the unannealed surfaces became more hydrophobic as demonstrated by contact angles above 60°. Such higher water contact angle values were likely due to a high degree of film roughness after placing under water (Table S2). The water contact angles of thermally annealed films were all hydrophobic before submersion and did not change significantly after submersion. The more consistent contact angle values before and after submersion are believed to be due to smaller changes in roughness values after submersion as compared to unannealed films.[46] These consistent contact angles also support the observation that through thermal annealing and the BBCP structure, we can produce more stable nanometer-scale morphologies. In comparison, amphiphilic linear BCP surfaces become hydrophilic after water immersion.[47,48] In this previous work, the hydrophilicity resulted from polymer reorganization to expose the hydrophilic polymers to water surfaces.[21,47,48] Thus, the resulting hydrophobic surfaces of our BBCP films upon water exposure were more likely due to the increase in the polymer surface roughness.

CONCLUSIONS

A versatile sequential polymerization of NB-PS and NB-PDMH provided a series of well-defined bottlebrush architectures that could generate asymmetric side-chain lengths and the desired f_{PDMH}. AFM images demonstrated distinct phase separation of the resultant BBCPs in thin films, and the phase-segregated morphologies could be manipulated by varying f_{PDMH}, the total DP, and polymer side-chain length asymmetry. Unannealed films demonstrated alteration of the self-assembled morphology, surface roughening, and the change in domain sizes after water submersion due to the polymer reconstruction from the swelling of the PDMH polymer segments and aggregation of the alkyl chain pendant groups and RAFT CTA alkyl chains. The thermal annealing method appeared to favor thermodynamic phase separation of the BBCP films, leading to an equilibrium morphology. After water submersion, the thermally annealed BBCP films with $f_{PDMH} \sim 0.5$ demonstrated a water-stable morphology, but the morphology was still unstable for the films with higher f_{PDMH}. Additionally, BBCP films became more hydrophobic due to the increase in surface roughness after water submersion. Thermally annealed films were initially more hydrophobic due to adopting a more equilibrium morphology prior to water submersion, and this hydrophobicity did not change significantly after water submersion due to their increased stability. Accordingly, the results suggest that the thermally annealed BBCP films with $f_{PDMH} \sim 0.5$ can be used for future antifouling and antimicrobial performance studies. Additionally, this system can generate high-density cationic BBCPs that can be utilized in a multitude of other coating applications.

ASSOCIATED CONTENT

Supporting Information

The Supporting Information is available free of charge at https://pubs.acs.org/doi/10.1021/acs.macromol.1c01161.

Measurement of thin-film thickness, ^{1}H NMR spectrum of NB-PS_{39}, SEC profiles of MMs, DSC chromatograms of homopolymers and BBCPs, plots of domain spacing as a function of overall DP, AFM images of unannealed BBCP films and thermally annealed films before and after water submersion, and water contact angle measurement (PDF)

AUTHOR INFORMATION

Corresponding Author

William M. Gramlich − *Department of Chemistry, University of Maine, Orono, Maine 04469, United States; Advanced Structures and Composites Center, University of Maine, Orono, Maine 04469, United States;* orcid.org/0000-0002-7040-6503; Email: william.gramlich@maine.edu

Authors

Hathaithep Senkum − *Department of Chemistry, University of Maine, Orono, Maine 04469, United States*

https://doi.org/10.1021/acs.macromol.1c01161
Macromolecules 2021, 54, 7987−7997

Peter V. Kelly − *Department of Chemistry, University of Maine, Orono, Maine 04469, United States*

Complete contact information is available at: https://pubs.acs.org/10.1021/acs.macromol.1c01161

Notes

The authors declare no competing financial interest.

■ ACKNOWLEDGMENTS

This research was supported by the Department of Chemistry at the University of Maine, the National Science Foundation award (#IIA-1355457) to Maine EPSCoR at the University of Maine, and UT-Battelle LLC with the U.S. Department of Energy under contract DE-AC05-00OR22725 (subcontract no. 4000174848). ^{1}H NMR characterization was performed on a Bruker Avance NEO 500 MHz nuclear magnetic resonance (NMR) spectrometer supported by the National Science Foundation under grant # CHE-1828408.

■ REFERENCES

(1) Xie, G.; Martinez, M. R.; Olszewski, M.; Sheiko, S. S.; Matyjaszewski, K. Molecular Bottlebrushes as Novel Materials. *Biomacromolecules* **2019**, *20*, 27−54.

(2) Warren, N. J.; Armes, S. P. Polymerization-Induced Self-Assembly of Block Copolymer Nano-objects via RAFT Aqueous Dispersion Polymerization. *J. Am. Chem. Soc.* **2014**, *136*, 10174−10185.

(3) Sankaran, N. B.; Rys, A. Z.; Nassif, R.; Nayak, M. K.; Metera, K.; Chen, B.; Bazzi, H. S.; Sleiman, H. F. Ring-Opening Metathesis Polymers for Biodetection and Signal Amplification: Synthesis and Self-Assembly. *Macromolecules* **2010**, *43*, 5530−5537.

(4) Hou, Z.; Ren, M.; Wang, K.; Yang, Y.; Xu, J.; Zhu, J. Deformable Block Copolymer Microparticles by Controllable Localization of pH-Responsive Nanoparticles. *Macromolecules* **2020**, *53*, 473−481.

(5) Lang, C.; Ye, D.; Song, W.; Yao, C.; Tu, Y.-M.; Capparelli, C.; LaNasa, J. A.; Hickner, M. A.; Gomez, E. W.; Gomez, E. D.; Hickey, R. J.; Kumar, M. Biomimetic Separation of Transport and Matrix Functions in Lamellar Block Copolymer Channel-Based Membranes. *ACS Nano* **2019**, *13*, 8292−8302.

(6) Ziemba, C.; Khavkin, M.; Priftis, D.; Acar, H.; Mao, J.; Benami, M.; Gottlieb, M.; Tirrell, M.; Kaufman, Y.; Herzberg, M. Antifouling Properties of a Self-Assembling Glutamic Acid-Lysine Zwitterionic Polymer Surface Coating. *Langmuir* **2019**, *35*, 1699−1713.

(7) Xie, Q.; Pan, J.; Ma, C.; Zhang, G. Dynamic surface antifouling: mechanism and systems. *Soft Matter* **2019**, *15*, 1087−1107.

(8) Bates, F. S.; Fredrickson, G. H. Block copolymer thermodynamics: theory and experiment. *Annu. Rev. Phys. Chem.* **1990**, *41*, 525−557.

(9) Fredrickson, G. H.; Bates, F. S. Dynamics of block copolymers: Theory and experiment. *Annu. Rev. Mater. Sci.* **1996**, *26*, 501−550.

(10) Urbas, A.; Sharp, R.; Fink, Y.; Thomas, E. L.; Xenidou, M.; Fetters, L. J. Tunable Block Copolymer/Homopolymer Photonic Crystals. *Adv. Mater.* **2000**, *12*, 812−814.

(11) Deng, T.; Chen, C.; Honeker, C.; Thomas, E. L. Two-dimensional block copolymer photonic crystals. *Polymer* **2003**, *44*, 6549−6553.

(12) Song, D. P.; Zhao, T. H.; Guidetti, G.; Vignolini, S.; Parker, R. M. Hierarchical Photonic Pigments *via* the Confined Self-Assembly of Bottlebrush Block Copolymers. *ACS Nano* **2019**, *13*, 1764−1771.

(13) Gai, Y.; Song, D.-P.; Yavitt, B. M.; Watkins, J. J. Polystyrene-*block*-poly(ethylene oxide) Bottlebrush Block Copolymer Morphology Transitions: Influence of Side Chain Length and Volume Fraction. *Macromolecules* **2017**, *50*, 1503−1511.

(14) Fenyves, R.; Schmutz, M.; Horner, I. J.; Bright, F. V.; Rzayev, J. Aqueous Self-Assembly of Giant Bottlebrush Block Copolymer Surfactants as Shape-Tunable Building Blocks. *J. Am. Chem. Soc.* **2014**, *136*, 7762−7770.

(15) Wang, Q.; Xiao, A.; Shen, Z.; Fan, X.-H. Janus particles with tunable shapes prepared by asymmetric bottlebrush block copolymers. *Polym. Chem.* **2019**, *10*, 372−378.

(16) Kerstetter, J. L.; Gramlich, W. M. Nanometer-scale self-assembly of amphiphilic copolymers to control and prevent biofouling. *J. Mater. Chem. B* **2014**, *2*, 8043−8052.

(17) Beyth, N.; Yudovin-Farber, I.; Bahir, R.; Domb, A. J.; Weiss, E. I. Antibacterial activity of dental composites containing quaternary ammonium polyethylenimine nanoparticles against Streptococcus mutans. *Biomaterials* **2006**, *27*, 3995−4002.

(18) Guo, J.; Qin, J.; Ren, Y.; Wang, B.; Cui, H.; Ding, Y.; Mao, H.; Yan, F. Antibacterial activity of cationic polymers: side-chain or main-chain type? *Polym. Chem.* **2018**, *9*, 4611−4616.

(19) Druvari, D.; Koromilas, N. D.; Lainioti, G. C.; Bokias, G.; Vasilopoulos, G.; Vantarakis, A.; Baras, I.; Dourala, N.; Kallitsis, J. K. Polymeric Quaternary Ammonium-Containing Coatings with Potential Dual Contact-Based and Release-Based Antimicrobial Activity. *ACS Appl. Mater. Interfaces* **2016**, *8*, 35593−35605.

(20) Martinelli, E.; Agostini, S.; Galli, g.; Chiellini, E.; Glisenti, A.; Pettitt, M. E.; Callow, M. E.; Callow, J. A.; Graf, K.; Bartels, f. W. Nanostructured Films of Amphiphilic Fluorinated Block Copolymers for Fouling Release Application. *Langmuir* **2008**, *24*, 13138−13147.

(21) Cho, Y.; Sundaram, H. S.; Weinman, C. J.; Paik, M. Y.; Dimitriou, M. D.; Finlay, J. A.; Callow, M. E.; Callow, J. A.; Kramer, E. J.; Ober, C. K. Triblock Copolymers with Grafted Fluorine-Free, Amphiphilic, Non-Ionic Side Chains for Antifouling and Fouling-Release Applications. *Macromolecules* **2011**, *44*, 4783−4792.

(22) Xia, Y.; Adibnia, V.; Huang, R.; Murschel, F.; Faivre, J.; Xie, G.; Olszewski, M.; De Crescenzo, G.; Qi, W.; He, Z.; Su, R.; Matyjaszewski, K.; Banquy, X. Biomimetic Bottlebrush Polymer Coatings for Fabrication of Ultralow Fouling Surfaces. *Angew. Chem., Int. Ed.* **2019**, *58*, 1308−1314.

(23) Roeven, E.; Kuzmyn, A. R.; Scheres, L.; Baggerman, J.; Smulders, M. M. J.; Zuilhof, H. PLL−Poly(HPMA) Bottlebrush-Based Antifouling Coatings: Three Grafting Routes. *Langmuir* **2020**, *36*, 10187−10199.

(24) Li, F.; Weir, M. D.; Xu, H. H. K. Effects of Quaternary Ammonium Chain Length on Antibacterial Bonding Agents. *J. Dent. Res.* **2013**, *92*, 932−938.

(25) Koufakis, E.; Manouras, T.; Anastasiadis, S. H.; Vamvakaki, M. Film Properties and Antimicrobial Efficacy of Quaternized PDMAEMA Brushes: Short vs Long Alkyl Chain Length. *Langmuir* **2020**, *36*, 3482−3493.

(26) Barnes, A. M.; Du, Y.; Zhang, W.; Seifert, S.; Buratto, S. K.; Coughlin, E. B. Phosphonium-Containing Block Copolymer Anion Exchange Membranes: Effect of Quaternization Level on Bulk and Surface Morphologies at Hydrated and Dehydrated States. *Macromolecules* **2019**, *52*, 6097−6106.

(27) Fultz, B. A.; Terlier, T.; Dunoyer de Segonzac, B.; Verduzco, R.; Kennemur, J. G. Nanostructured Films of Oppositely Charged Domains from Self-Assembled Block Copolymers. *Macromolecules* **2020**, *53*, 5638−5648.

(28) Weber, R. L.; Ye, Y.; Schmitt, A. L.; Banik, S. M.; Elabd, Y. A.; Mahanthappa, M. K. Effect of Nanoscale Morphology on the Conductivity of Polymerized Ionic Liquid Block Copolymers. *Macromolecules* **2011**, *44*, 5727−5735.

(29) Senkum, H.; Gramlich, W. M. Cationic Bottlebrush Polymers from Quaternary Ammonium Macromonomers by Grafting-Through Ring-Opening Metathesis Polymerization. *Macromol. Chem. Phys.* **2020**, *221*, 1900476.

(30) Turgut, H.; Dingenouts, N.; Trouillet, V.; Krolla-Sidenstein, P.; Gliemann, H.; Delaittre, G. Reactive block copolymers for patterned surface immobilization with sub-30 nm spacing. *Polym. Chem.* **2019**, *10*, 1344−1356.

(31) Seo, H.-B.; Yu, Y.-G.; Chae, C.-G.; Kim, M.-J.; Lee, J.-S. Synthesis of Ultrahigh Molecular Weight Bottlebrush Block

Copolymers of ω-end-norbornyl polystyrene and polymethacrylate macromonomers. *Polymer* **2019**, *177*, 241−249.
(32) Sutthasupa, S.; Shiotsuki, M.; Sanda, F. Recent advances in ring-opening metathesis polymerization, and application to synthesis of functional materials. *Polym. J.* **2010**, *42*, 905−915.
(33) Yu, Y.-G.; Seo, C.; Chae, C.-G.; Seo, H.-B.; Kim, M.-J.; Kang, Y.; Lee, J.-S. Hydrogen Bonding-Mediated Phase Transition of Polystyrene and Polyhydroxystyrene Bottlebrush Block Copolymers with Polyethylene Glycol. *Macromolecules* **2019**, *52*, 4349−4358.
(34) Geol, V.; Beginn, U.; Mourran, A.; Moller, M. 'Quat-Primer' Polymers Bearing Cationic and Reactive Groups: Synthesis, Characterization, and Application. *Macromolecules* **2008**, *41*, 8187−8197.
(35) Dizman, B.; Elasri, M. O.; Mathias, L. J. Synthesis and Characterization of Antibacterial and Temperature Responsive Methacrylamide Polymers. *Macromolecules* **2006**, *39*, 5738−5746.
(36) Rahman, S. S. A.; Kawaguchi, D.; Ito, D.; Takano, A.; Matsushita, Y. Phase behavior of poly(4-*tert*-butylstyrene-*stat*-4-*tert*-butoxystyrene)/polyisoprene blends with competitive interactions. *J. Polym. Sci., Part B: Polym. Phys.* **2009**, *47*, 2272−2280.
(37) Runge, M. B.; Lipscomb, C. E.; Ditzler, L. R.; Mahanthappa, M. K.; Tivanski, A. V.; Bowden, N. B. Investigation of the Assembly of Comb Block Copolymers in the Solid State. *Macromolecules* **2008**, *41*, 7687−7694.
(38) Ji, E.; Cummins, C.; Fleury, G. Precise Synthesis and Thin Film Self-Assembly of PLLA-b-PS Bottlebrush Block Copolymers. *Molecules* **2021**, *26*, 1412−1422.
(39) Yang, Q.; Loos, K. Perpendicular Structure Formation of Block Copolymer Thin Films during Thermal Solvent Vapor Annealing: Solvent and Thickness Effects. *Polymers* **2017**, *9*, 525−535.
(40) Ningrum, E. O.; Lin, W.-T.; Lo, C.-T. The Nanostructure and Dewetting of Block Copolymer Thin Films Annealed in different Neutral Solvent. *Polym. Eng. Sci.* **2011**, *51*, 1339−1346.
(41) Di, C.-A.; Yu, G.; Liu, Y.; Guo, Y.; Sun, X.; Zheng, J.; Wen, Y.; Wang, Y.; Wu, W.; Zhu, D. Effect of dielectric layers on device stability of pentacene-based field-effect transistors. *Phys. Chem. Chem. Phys.* **2009**, *11*, 7268−7273.
(42) Theato, P.; Brehmer, M.; Conrad, L.; Frank, C. W.; Funk, L.; Yoon, D. Y.; Lüning, J. Surface Reorganization of an Amphiphilic Block Copolymer Film Studied by NEXAFS Spectroscopy. *Macromolecules* **2006**, *39*, 2592−2595.
(43) He, Y.; Wan, X.; Lin, W.; Li, J.; Li, Z.; Luo, F.; Li, J.; Tan, H.; Fu, Q. The synergistic effect of hierarchical structure and alkyl chain length on the antifouling and bactericidal properties of cationic/zwitterionic block polymer brushes. *Biomater. Sci.* **2020**, *8*, 6890−6902.
(44) Paul, D. K.; Karan, K. Conductivity and Wettability Changes of Ultrathin Nafion Films Subjected to Thermal Annealing and Liquid Water Exposure. *Phys. Chem. C* **2014**, *118*, 1828−1835.
(45) Borodinov, N.; Belianinov, A.; Chang, D.; Carrillo, J.-M.; Burch, M. J.; Xu, Y.; Hong, K.; Ievlev, A. V.; Sumpter, B. G.; Ovchinnikova, O. S. Molecular reorganization in bulk bottlebrush polymers: direct observation *via* nanoscale imaging. *Nanoscale* **2018**, *10*, 18001−18009.
(46) Xu, Y.; Wang, W.; Wang, Y.; Zhu, J.; Uhrig, D.; Lu, X.; Keum, J. K.; Mays, J. W.; Hong, K. Fluorinated bottlebrush polymers based on poly(trifluoroethyl methacrylate): synthesis and characterization. *Polym. Chem.* **2016**, *7*, 680−688.
(47) Martinelli, E.; Galli, G.; Cwikel, D.; Marmur, A. Wettability and Surface Tension of Amphiphilic Polymer Films: Time-Dependent Measurements of the Most Stable Contact Angle. *Macromol. Chem. Phys.* **2012**, *213*, 1448−1456.
(48) Cho, Y.; Sundaram, H. S.; Finlay, J. A.; Dimitriou, M. D.; Callow, M. E.; Callow, J. A.; Kramer, E. J.; Ober, C. K. Reconstruction of Surfaces from Mixed Hydrocarbon and PEG Components in Water: Responsive Surfaces Aid Fouling Release. *Biomacromolecules* **2012**, *13*, 1864−1874.

https://doi.org/10.1021/acs.macromol.1c01161
Macromolecules 2021, 54, 7987−7997